

NO computations in natural gas engines using a modified reaction-rate-controlled NO model

S. M. Aithal

Argonne National Laboratory

9700 S. Cass Ave., Argonne, IL 60439, USA

Phone # 630-252-3164, e-mail: aithal@mcs.anl.gov

Abstract: Development of computationally fast, numerically robust, and accurate models to compute engine-out NO emissions can play an important role in the design, development, and optimization of automotive engines fueled by alternative fuel blends. Detailed multidimensional models that couple fluid dynamics and chemical kinetics place stringent demands on the computational resources and time, precluding their use in design and parametric studies. This work describes the development of an integrated design tool which couples a fast, robust, physics-based, two-zone quasi-dimensional engine model with a modified reaction-rate-controlled NO model. This integrated design tool was used to study the engine-out NO in a natural gas engine. Engine-out NO predicted by this integrated design tool compared well with experimental data for a large range of equivalence ratios. The results of this work highlighted some of the possible deficiencies of using the two-zone model for engine-out NO predictions at low equivalence ratios.

Keywords: modified Heywood model, NO, emissions, natural gas, two-zone model

Nomenclature

A surface area of cylinder head (m^2)

$a_{n,k}$	coefficients fits to thermodynamic data of k^{th} species
$C_{p,k}$	molar heat capacity at constant pressure of the k^{th} species (J/mole-K)
$C_{v,k}$	molar heat capacity at constant volume of the k^{th} species (J/mole-K)
\bar{c}_p	mixture-averaged molar specific heat at constant pressure (J/mole-K)
\bar{c}_v	mixture-averaged molar specific heat at constant volume (J/mole-K)
h_{cg}	convective heat transfer coefficient $W\ m^{-2}\ K$
H_k	molar enthalpy of the k^{th} species (J/mole)
H_P	enthalpy of the products (J)
H_R	enthalpy of the reactants (J)
m	instantaneous mass in the engine cylinder (kg)
m_{fb}	mass of fuel (kg)
N_{rpm}	rotational speed of the engine (rev/min)
$P(\theta)$	average cylinder pressure at crank angle θ (N/m^2)
Q_{in}	heat input from fuel combustion (J)
Q_{loss}	heat lost from engine cylinder (J)
R_g	gas constant (J/kg-K)
R_u	universal gas constant (J/K)
$T(\theta)$	average cylinder temp at crank angle θ (K)
T_w	wall temperature (K)
U_k	molar internal energy of the k^{th} species (J/mole)
$V(\theta)$	instantaneous volume at crank angle θ
$x_1(\theta)$	distance of cylinder head from TDC at θ
X_k	mole fraction of the k^{th} species

Greek Symbols

γ	ratio of specific heats
θ	crank angle
ϕ	equivalence ratio
ω	engine speed ($= 6N_{rpm}$ deg/sec)

Abbreviations

ATDC	after top dead center
BDC	bottom dead center
CAD	crank angle degrees
EOC	end of combustion
EVO	exhaust valve open
LHV	lower heating value
RHS	right-hand side
SI	spark ignition
SOI	start of ignition
TDC	top dead center

1 Introduction

The use of natural gas as a fuel for internal combustion engines (ICEs) has received renewed attention, because of its clean burning characteristics and lower price as compared with petroleum derivatives. Natural gas vehicles can achieve up to 93 percent reduction in carbon monoxide emissions, 33 percent reduction in emissions of various oxides of nitrogen, and 50 percent reduction in reactive hydrocarbons when compared with gasoline vehicles. Natural gas vehicles also have greatly reduced emissions of particulate matter. Furthermore, since methane

does not readily ignite, it can be used in engines with a compression ratio as high as 12:1, thus resulting in greater thermal efficiency. Motivated by these advantages, researchers have conducted various experimental and numerical studies investigating the performance and emission characteristics of natural gas engines [1-8]. One particularly important example is the use of natural gas in stationary large-bore engines in applications such as power generation and gas transmission. Since such engines are used for long durations, optimizing their performance and emissions is essential. Detailed experimental and numerical investigations are required for the design and development of such engines.

Conducting a transient multidimensional numerical simulation of the entire engine cycle consisting of intake, compression, power, and exhaust strokes is a daunting computational task. Such simulations can take several hours to days, depending on the availability of computational power, complexity of the flow or chemistry model, and size of the computational domain. Hence, the required computational effort precludes its use in early stages of design, development, and engine optimization in terms of performance and emissions. Computationally fast, robust, physics-based, quasi-dimensional modeling tools, on the other hand, require minimal computational resources, and the computational time for solutions is usually on the order of seconds. Development of such quasi-dimensional modeling tools can greatly aid the design, analysis, and optimization of engines powered with alternative fuels such as natural gas. Such design tools can also be used for comparing the efficacy of various NO_x reduction techniques. Experimental studies are useful in validating and calibrating numerical models [9-11]. These numerical models in turn can be used to examine a range of operating conditions (cylinder pressure, RPM, compression ratio, equivalence ratio) and other emission-reducing technologies (catalysts, EGR, etc.), thus complementing experimental efforts.

To this end, we present here a computationally fast, numerically robust, physics-based integrated tool to compute engine-out NO in spark-ignited engines. This integrated tool couples a two-zone quasi-dimensional engine model to compute the temporal variation of engine pressure and temperatures (burned and unburned) with a modified reaction-rate controlled NO model proposed in [12]. The modified reaction-rate-controlled model discussed in [12] is an extension of the rate-controlled NO model proposed by Heywood [13]. Computation of engine-out NO based on the rate-controlled model requires the equilibrium concentration of the products of combustion at each crank angle in the engine cycle. Computation of these equilibrium concentrations can be very computationally expensive and cumbersome. To reduce the computational expense of computing the equilibrium composition of various combustion products, the two-zone quasi-dimensional model was coupled with a previously developed, fast, robust solver to compute equilibrium composition of combusting mixtures [14]. As an example, this integrated design tool was used to compute the engine-out NO in a spark-ignited natural gas engine. Results show that engine-out NO predicted using this numerical tool compares well with experimental data. Moreover, the methodology of coupling a quasi-dimensional engine model to NO computations proposed in this work can be extended to single and multizone diesel engines as well.

This paper is organized as follows. Section 2 discusses the two-zone quasi-dimensional model and the modified rate-controlled NO model. Section 3 discusses the method of solution. Section 4 discusses important results from the quasi-dimensional engine model and the modified NO model. Section 5 presents important conclusions and observations about this work.

2 Mathematical Formulation

This section describes the two-zone quasi-dimensional model used to compute the temporal variation of the average cylinder pressure along with the burned and unburned gas temperature in a spark-ignited engine. The modified reaction rate-controlled NO model is also described in this section.

2.1 Two-Zone Model for Computing Temporal Variations of Temperature and Pressure

A numerical model used to compute the temporal variation of temperature and pressure in a single-cylinder diesel engine was described in detail in Ref. [15]. A similar methodology was used in this work to model a spark-ignited, large-bore natural gas engine. Temporal variation of the engine pressure and temperature during the compression and power stroke was obtained by a numerical solution of the energy equation as in Ref. [15]. Effects of temperature and mixture composition on the thermophysical properties of the working fluid were included in the solution of the energy equation. Temporal variations of the thermophysical properties of all the species in the gas mixture were obtained by using thermodynamic coefficients from the CHEMKIN database. Following the procedure in Ref. [15], fuel combustion chemistry was modeled by a single-step global reaction. The combustion process of the premixed fuel-air mixture after the spark was modeled by using the well-known Wiebe function. The Wiebe function can be used to compute the mass of fuel burned at each crank angle and also the burned and unburned gas temperature.

The energy equation describing the variation of pressure with crank angle is as follows.

$$\frac{dP(\theta)}{d\theta} = \frac{\gamma - 1}{V(\theta)} (Q_{in} - Q_{loss}) - \gamma \frac{P(\theta)}{V(\theta)} \frac{dV}{d\theta} \quad (1)$$

The amount of heat produced (Q_{in}) due to the fuel burned ($m_{fb}(\theta)$) from θ and $\theta+d\theta$ is given by

$$Q_{in}(\theta) = (H_p(T) - H_R(T)) \cong m_{fb}(\theta) LHV \quad , \quad (2)$$

while the heat lost from the engine during the interval is given by

$$Q_{loss}(\theta) = \frac{h_{cg} A}{\omega} (T(\theta) - T_w) \quad . \quad (3)$$

The instantaneous values of volume, area, and displacement given by the slider-crank model [15] are as follows.

$$V(\theta) = V_c + \frac{\pi D^2}{4} x_1(\theta) \quad (4)$$

$$A(\theta) = 2 \left(\frac{\pi D^2}{4} \right) + \pi D x_1(\theta) \quad (5)$$

$$x_1(\theta) = (l + R) - \left[R \cos \theta + \sqrt{(l^2 - R^2 \sin^2 \theta)} \right] \quad (6)$$

The convective heat transfer coefficient is expressed as

$$h_{cg} = 3.26 D^{-0.2} P^{0.8} T^{-0.55} w^{0.8} \quad , \quad (7)$$

where the velocity of the burned gas w is given by

$$w = c_1 S_p + c_2 \frac{V_d T_r}{p_r V_r} (P(\theta) - P_m) \quad . \quad (8)$$

Specific heats, enthalpies, and internal energy of individual species in the working fluid were computed by using polynomials as follows.

$$\frac{C_{p,k}}{R_u} = a_{1,k} + a_{2,k} T + a_{3,k} T^2 + a_{4,k} T^3 + a_{5,k} T^4 \quad (9)$$

$$C_{v,k} = C_{p,k} - R_u \quad (10)$$

$$H_k = \left(a_{1,k} + \frac{a_{2,k}}{2} T + \frac{a_{3,k}}{3} T^2 + \frac{a_{4,k}}{4} T^3 + \frac{a_{5,k}}{5} T^4 + \frac{a_{6,k}}{T} \right) R_u T \quad (11)$$

$$U_k = H_k - R_u T \quad (12)$$

Mixture-averaged values of specific heat of the working fluid were averaged by using mole fractions as follows.

$$\begin{aligned} \overline{C_v} &= \sum_{k=1}^K X_k C_{v,k}; & \overline{C_p} &= \sum_{k=1}^K X_k C_{p,k} \\ \gamma &= \frac{\overline{C_p}}{\overline{C_v}} \end{aligned} \quad (13)$$

A similar procedure was used to compute the mixture-averaged values of enthalpy and internal energy of the working fluid.

The Wiebe function was used to compute the burned mass fraction as shown below [13],

$$x_b(\theta) = \frac{m_{fb}}{m_{fT}} = \left\{ 1 - \exp \left\{ -a \left(\frac{\theta - \theta_0}{\theta_b} \right)^{m+1} \right\} \right\} , \quad (14)$$

where θ , θ_0 , and θ_b are the instantaneous crank angle, the crank angle for the start of combustion, and the combustion duration, respectively. Further, m_{fb} is the fuel burned; m_{fT} is the total fuel at BDC; and $x_b(\theta) - x_b(\theta - 1)$ is the fraction of fuel burned in each crank angle and is used to compute Q_{in} in Eq. (2).

The average gas temperature was obtained as

$$T(\theta) = \frac{P(\theta)V(\theta)}{m(\theta)R_g} . \quad (15)$$

The burned and unburned gas temperature were obtained as

$$T_b(\theta) = \frac{P(\theta)V_b(\theta)}{m_b(\theta)R_{gb}} , \quad (16)$$

$$T_u(\theta) = \frac{P(\theta)V_u(\theta)}{m_u(\theta)R_{gu}} , \quad (17)$$

where the subscripts “u” and “b” represent unburned and burned quantities, respectively. The volume fraction of the burned gas $y_b (=V_b/V)$ can be obtained by using the following relationship [13].

$$x_b(\theta) = \left[1 + \frac{\rho_u}{\rho_b} \left(\frac{1}{y_b} - 1 \right) \right]^{-1} \quad (18)$$

Following Ref. [13], $\frac{\rho_u}{\rho_b} = 4.0$ was used for the sake of simplicity.

The moles of CO_2 , H_2O , O_2 , and N_2 produced in CAD $d\theta$ in accordance with the single-step global chemistry model are as follows.

$$n_{\text{CO}_2}(d\theta) = x_1(x_b(\theta) - x_b(\theta - d\theta)) / M_{\text{CH}_4} \quad (19)$$

$$n_{\text{H}_2\text{O}}(d\theta) = \frac{y_1}{2}(x_b(\theta) - x_b(\theta - d\theta)) / M_{\text{CH}_4} \quad (20)$$

$$n_{\text{O}_2}(d\theta) = \left(\frac{1}{\phi} - 1 \right) \left(x_1 + \frac{y_1}{4} \right) (x_b(\theta) - x_b(\theta - d\theta)) / M_{\text{CH}_4} \quad (21)$$

$$n_{\text{N}_2}(d\theta) = \left(\frac{\beta}{\phi} \right) \left(x_1 + \frac{y_1}{4} \right) (x_b(\theta) - x_b(\theta - d\theta)) / M_{\text{CH}_4} \quad (22)$$

In Eqs. (19) through (22), $x_1 = 1$ and $y_1 = 4$ for methane; β is the $\text{N}_2:\text{O}_2$ ratio in air, which is taken to be 3.76 and M_{CH_4} is the molecular mass of methane.

The total number of moles of any specie (CO_2 , H_2O , O_2 , and N_2) in the burned zone at any crank angle θ is

$$n_N(\theta) = \sum_{\theta = \theta_i}^{\theta = \theta_f} n_N(d\theta) \quad , \quad (23)$$

where the summation is over the crank angle interval from θ_i (SOI) to θ . Since the initial moles of fuel, O_2 , and N_2 are known, the composition of the unburned zone can be computed based on Eqs. (19)–(23).

2.2 Modified Rate-Controlled NO Model

The extended Zeldovich mechanism is used to derive a rate expression for the time rate of change of NO concentration; for details, see [13]. Table 1 shows the reactions in the extended Zeldovich mechanism (units cm^3 , gmol, s, K) where, K_i^+ and K_i^- represent the forward and backward reaction rates of the i th reaction ($i = 1, 2$, or 3). Based on the extended Zeldovich mechanism, the expression for the time rate of change of NO is as follows.

$$\begin{aligned} \frac{d[NO]}{dt} = & k_1^+ [O][N_2] + k_2^+ [N][O_2] + k_3^+ [N][OH] \\ & - k_1^- [NO][N] - k_2^- [NO][O] - k_3^- [NO][H] \end{aligned} \quad (24)$$

This expression is simplified by using two main assumptions: (1) the C-O-H system is in equilibrium and is unaffected by N_2 dissociation, and (2) atomic nitrogen (N atoms) change concentration by a quasi-steady process [16]. The first assumption implies that the concentrations of O, O_2 , H, OH, and N_2 in Eq. (24) can be approximated by their equilibrium concentrations at a given temperature and pressure. The second assumption implies that the rate

of change of the atomic nitrogen concentration is zero, $\frac{d[N]}{dt} \cong 0$

Equation (25) shows the time rate of change of the atomic nitrogen [N] concentration.

$$\frac{d[N]}{dt} = k_1^+ [O][N_2] - k_2^+ [N][O_2] - k_3^+ [N][OH] - k_1^- [NO][N] + k_2^- [NO][O] + k_3^- [NO][H] \quad (25)$$

Since $\frac{d[N]}{dt} \cong 0$, Eq. (25) can be simplified to obtain [N].

$$[N] = \frac{k_1^+ [O][N_2] + k_2^- [NO][O] + k_3^- [NO][H]}{k_3^+ [OH] + k_1^- [NO] + k_2^+ [O_2]} \quad (26)$$

Adding Eq. (24) and Eq. (25), $\frac{d[NO]}{dt}$ can be simplified to obtain the following.

$$\frac{d[NO]}{dt} = 2k_1^+ [O][N_2] - 2k_1^- [NO][N] \quad (27)$$

The concentration of O, N₂, NO, H, OH and O₂ are used in computing the RHS of Eq. (26) and Eq. (27). The rate-controlled model for NO described above is sometimes referred to as the Heywood model. The rate constants and equilibrium concentrations of species used in evaluating Eq. (27) are computed by using the burned gas temperature and pressure at a given crank angle. Effects of mixing between the burned and unburned gas and the temperature gradients in the burned gas region are neglected. Solution of Eq. (27) yields the temporal variation of NO concentration (in moles/cm³).

Solution of Eq. (27) reveals that a few CAD after the end of combustion (typically about 30–50 ATDC) the NO concentration (defined as moles per volume) is constant until EVO. The fact that the NO concentration remains fixed implies that the total moles of NO increase during the later portion of the expansion cycle (the cylinder volume is increasing during the expansion stroke). This behavior is unphysical, however, since the cylinder temperature, pressure, and species number densities are all monotonically decreasing during the expansion stroke, thus precluding the monotonic increase of NO moles (net increased production of NO). Indeed, it is well accepted that the total moles (not concentration) of NO are frozen during the later portion of the expansion cycle. This incorrect prediction of the temporal variation of NO moles is due the fact that Eq. (27) does not account for the change in burned zone volume. Ref. [12] discusses an

extension of Eq. (27) to include the effect of burned zone volume. Since $[NO] = \frac{N_{NO}}{V}$, where

N_{NO} is the number of moles of NO, the LHS of Eq. (27) can be rewritten as

$$\frac{d[NO]}{dt} = \frac{d}{dt} \left[\frac{N_{NO}}{V} \right] = \frac{1}{V} \frac{dN_{NO}}{dt} + \frac{d}{dt} \left(\frac{1}{V} \right) N_{NO}, \quad (28)$$

which can be shown to yield

$$\frac{d[NO]}{dt} = \left. \frac{d[NO]}{dt} \right|_H - [NO] \frac{1}{V_b} \frac{dV_b}{dt}, \quad (29)$$

where $\left. \frac{d[NO]}{dt} \right|_H$ is the rate of change of NO concentration at constant volume (Heywood model) computed by using Eq. (27). The second term on the RHS of Eq. (29) accounts for the decrease in NO concentration as a result of increasing cylinder volume during the expansion stroke.

From SOC to EOC, the burned volume V_b can be computed based on the procedure discussed earlier. After EOC, $V_b = V(\theta)$, where $V(\theta)$ is the cylinder volume at crank angle θ . Equation (29) is referred to as the modified rate-controlled NO model because it accounts for the rate of change of the engine volume in the determining the NO concentration during the engine cycle.

3 Method of Solution

The numerical model described above was used to compute the average pressure, temperature, and engine-out NO in a single-cylinder natural gas engine described in [7]. Methane was used as a surrogate for natural gas in all simulations for the sake of simplicity. The numerical procedure to obtain the cylinder pressure in a diesel engine is explained in detail in [15]. The same procedure was adapted to obtain the pressure and temperature in an SI engine using the equations described above. Briefly, for a given set of operating conditions, namely, the prescribed mass of

the fuel-air mixture and temperature at BDC, Eq. (1) was solved iteratively by using Eqs. (2)–(14) to obtain the pressure from $-179^\circ < \theta < 180^\circ$, in increments of 1° . For a given pressure at a crank angle, the burned and unburned gas temperatures were obtained by using Eqs. (14) and (15).

The engine dimensions and operating conditions used in this work were the same as those described in [7]. Table 2 shows the engine dimensions used in this work, and Table 3 shows the operating conditions.

The mass of the fuel (methane in this case) was kept constant at 0.13 g. A Weibe function with $a = -4$ and $m = 2$ was used to describe the rate of fuel combustion; see Eq. (14). The combustion duration (θ_b) used in Eq. (14) was chosen such that the peak pressure matched those reported in Ref. [7]. The spark timings for various ϕ were also obtained from Ref. [7]. In the two-zone model, it was assumed that no mixing occurred between the burned and unburned zones. The burned zone comprised CO_2 , H_2O , excess O_2 , and the corresponding amount of N_2 , whereas the unburned zone comprised the unburned fraction of fuel, O_2 , and N_2 . Equations (19)–(23) explain the procedure to compute the composition of the burned zone.

Knowing the temporal variation of temperature, pressure, and composition of the burned zone, one can compute the temporal variation of NO using Eq. (29). The solution of this equation requires computing equilibrium concentrations of O, N, OH, H, O_2 , and N_2 at every crank angle. For this purpose, we used a fast, accurate, and robust solver based on the equilibrium constant method that we had previously developed [14].

4 Results and Discussion

This section discusses the results of the quasi-dimensional model and the modified Heywood model. NO predictions using the modified Heywood model are compared with experimental data reported in Ref. [7] for various equivalence ratios.

4.1 Results from the Quasi-Dimensional Model

Figure 1 shows a comparison between the temporal variation of cylinder pressure obtained with the quasi-dimensional model discussed in Section 2 and experimental data (for $\phi = 0.9$). One can see that the cylinder pressure is well predicted by the quasi-dimensional model.

Figure 2 shows the typical temporal variation of the burned and unburned gas temperatures along with the single-zone (average) temperature distribution (also for $\phi = 0.9$). Until the start of ignition, the unburned gas temperature is characterized by a single-gas temperature, which is computed by using Eq. (15). After the start of combustion, the burned zone has a temperature in excess of 2500 K, whereas the unburned gas temperature follows the temperature rise expected from the isentropic compression.

Figure 3 shows the variation of the normalized burned and unburned zone volumes along with the total cylinder volume as a function of crank angle. All volumes were normalized with respect to the clearance volume. At the start of combustion, the volume of the unburned gas equals the total cylinder volume, whereas the burned volume is zero. As combustion proceeds, the burned-gas volume rises, slowly at first during the ignition delay period, followed by a more rapid rise. When the combustion is almost complete, the unburned-gas volume tends to zero while the burned-gas volume tends to the total instantaneous cylinder volume, as expected. Figure 3 also shows that for $-25^\circ < \theta < 25^\circ$, the cylinder volume does not change much, but for $\theta > 25^\circ$ (not shown in Figure 3) it increases rapidly as dictated by the Eq. (4).

Figure 4 shows the temporal variation of moles of CH_4 , O_2 , CO_2 , and H_2O as a function of crank-angle (for $\phi = 0.9$). Moles of all species were normalized with the initial fuel moles. Before SOC, the initial mixture contains 1 mole of CH_4 and 2.2 moles of O_2 along with 8.272 moles of N_2 (normalized values). The figure also shows that during combustion from -24 CAD to about 25 CAD, CH_4 and O_2 are depleted as dictated by Eq. (14) with the simultaneous formation of CO_2 and H_2O . As expected, after complete combustion of one mole of fuel (CH_4) with 2 moles of O_2 , one mole of CO_2 and 2 moles of H_2O are formed. About 0.2 moles of O_2 remain in the burned mixed after complete combustion (since $\phi = 0.9$).

Figure 1 through Figure 4 demonstrate the correct implementation of the two-zone model used in this work. The temporal variation of temperature and pressure obtained from the two-zone model was used to compute NO using Eq. (29). NO predictions using the modified Heywood model for various equivalence ratios are discussed next. The results compare well with experimental data reported in Ref. [7].

4.2 Results for the Modified Heywood Model

Evaluating the temporal variation of NO using the modified Heywood model (and also the Heywood model) requires computing the equilibrium composition of the combustion products in the fuel-air mixture. A fast, robust solver based on the equilibrium constant method was coupled to the quasi-dimensional engine model. Table 4 shows a comparison of mole fractions of various combustion products obtained using the equilibrium solver developed in Ref. [14] with computations using an equilibrium solver in [17]. The equilibrium compositions shown in Table 4 correspond to a particular temperature and pressure ($T = 2978 \text{ K}$, $P = 53.54 \text{ atm}$) in the burned-gas zone and verify the accuracy of the equilibrium solver used in this work.

Figure 5 shows the variation of the moles of CO₂, H₂O, excess oxygen, and nitrogen in the burned-gas zone in accordance with Eqs. (19)–(23). The number of moles of CO₂, H₂O, O₂, and N₂ at a given instant of time was used to compute the elemental composition of C, O, H, and N. The elemental composition along with the temperature and pressure at a given composition is required in order to compute the equilibrium composition of the combustion products as discussed in Ref. [14].

Figure 6 shows a comparison of the NO concentration (moles/m³) obtained by using the original Heywood model, Eq. (27), and the modified Heywood model, Eq. (29), for the case of $\phi = 0.9$. NO concentration obtained from equilibrium chemistry is also shown for comparison. One can see that the NO concentration predicted by the Heywood model reaches a steady value after about CAD 50, whereas the modified Heywood model shows that the NO concentration drops monotonically during the expansion stroke. The NO concentration predicted by equilibrium chemistry decreases monotonically during the expansion cycle as the cylinder temperature and pressure drop. The drop in the NO concentration predicted by equilibrium chemistry is more pronounced as compared to the modified rate-controlled NO model during the later portion of the expansion cycle, as expected.

Figure 7 shows the mole fraction of NO (expressed as PPM) for the original Heywood model and the modified model. Since the total moles (and hence NO mole fraction) is a product of NO concentration (in moles/m³) and cylinder volume at a given crank angle, the original Heywood model predicts a monotonic rise in NO (ppm) with crank angle after EOC, whereas the modified Heywood model correctly predicts that NO (PPM) remains constant after EOC. One can see that for crank angles close to TDC, the NO mole fractions predicted by the modified Heywood model and by the original Heywood model are close, whereas they start to deviate

significantly after about 50 CAD. The reason is that the effect of the volume correction near TDC is small but increases considerably after EOC when the burned gas volume equals the total cylinder volume.

Figure 8 shows the temporal variation of NO mole fraction for a range of equivalence ratios using the modified Heywood model. One can see that for all the equivalence ratios, the total NO mole fraction remains constant a few crank angle degrees after EOC, as expected.

Figure 9 shows a comparison of engine-out NO predicted by the modified Heywood model with experimental data reported in Ref. [7]. The prediction of the modified Heywood model matches the experimental data well for $0.8 < \phi < 1.0$. For $\phi < 0.8$, however, the predicted NO is higher than experimentally observed engine-out NO. This difference can be attributed to the fact that the two-zone model used in this work does not include the effects of mixing and temperature gradients in the burned zone. Table 3 shows that the combustion duration for $\phi < 0.8$ is much higher than for $\phi > 0.8$. The larger combustion duration could lead to more mixing with gases from the unburned zone and thus lowering the overall temperature of the burned-gas zone, leading to a lower value of engine-out NO.

The computational time required to obtain the NO concentration for any given equivalence ratio was about 100 milliseconds on a single core Intel 2.53 GHz machine. Since the computing time is on the order of 2–3 engine cycles, the numerical tool discussed in this work could have important applications in real-time engine control. The tool can also be used to simulate emission characteristics for a large number of cycles with varying driving conditions such as engine speed and load (such as the Federal Test Procedure cycles), thus greatly enhancing the utility of the tool discussed in this work.

5 Conclusions

This work focused on coupling a two-zone quasi-dimensional engine model with a modified rate-controlled NO model that addresses the deficiencies in the Heywood model. The coupled model predictions for engine-out NO from a natural gas engine compare well with engine data over a large range of equivalence ratios. The discrepancy between predicted and observed engine-out NO values at lower values of equivalence ratios is likely due to the effects of mixing that become important for large combustion duration. Increased mixing between the burned and unburned zones can lead to lower temperatures of the burned gases and hence lower NO at lower equivalence ratios.

Acknowledgments: This work was supported by the U.S. Department of Energy, under Contract DE-AC02-06CH11357.

References

1. Reynolds, C. C. O. B., Evans, R. L., "Improving emissions and performance characteristics of lean burn natural gas engines through partial stratification", *International Journal of Engine Research*, February 1, 2004, Vol.(5) 1 pp-105-114.
2. Goto, Y., "Development of a liquid natural gas pump and its application to direct injection liquid natural gas engines", *International Journal of Engine Research*, April 1, 2002; Vol. (3) No. 2, pp. 61-68.

3. Mbarawaa, M., Milton, B. E., Casey, R. T., "Experiments and modelling of natural gas combustion ignited by a pilot diesel fuel spray", *International Journal of Thermal Sciences*, Vol. 40 (10), 2001, pp. 927–936.
4. Ibrahim, A., Bari, S., "A comparison between EGR and lean-burn strategies employed in a natural gas SI engine using a two-zone combustion model", *Energy Conversion and Management* Vol. 50 (12), 2009, pp. 3129–3139.
5. Kesgin, U., "Study on prediction of the effects of design and operating parameters on NO_x emissions from a lean burn natural gas engine", *Energy Conversion and Management* Vol. 44 (6), 2003, pp. 907–921.
6. Abd Alla, G. H., Soliman, H. A., Badr, O. A., Abd Rabbo, M. F., "Combustion quasi-two zone predictive model for dual fuel engines", *Energy Conversion and Management* Vol. 42 (12), 2001, pp. 1477–1498.
7. Biruduganti, M., Gupta, S., Bihari, B., McConnell, S., Sekar, R., "Air separation membranes – an alternative to EGR in large bore natural gas engines," *ASME Internal Combustion Engine 2009*, Spring technical conference paper ICES2009-76054, 2009.
8. Ma, F., Wang, J., Wang, Y., Wang, Y., Li Y., Liu, H., and Ding, S., "Influence of Different Volume Percent Hydrogen/Natural Gas Mixtures on Idle Performance of a CNG Engine", *Energy Fuels*, 2008, 22 (3), pp 1880–1887.
9. Singh S. Reitz RD, Musculus MPB. "Comparison of the characteristic time (CTC), representative interactive flamelet (RIF), and direct integration with detailed chemistry models against optical diagnostic data for multi-mode combustion in a heavy-duty DI diesel engine". *SAE paper 2006-01-0055*, 2006.

10. Hildenbrand F, Schulz C, Wolfrum J, Keller F and Wagner E. 2000. "Laser diagnostic analysis of NO formation in a direct injection diesel engine with pump-line-nozzle and common rail injection systems". Proceedings of the Combustion Institute Vol. 28(1),pp 1137-1143.
11. Kashdan J. and Papagni J. LIF Imaging of Auto-ignition and Combustion in a Direct Injection Diesel-fuelled HCCI Engine. SAE Technical Paper 2005-01-3739.
12. Andersson, I., Eriksson, L., "A parametric model for ionization current in a four stroke SI engine", J. Dynamic Systems, Measurement and Control, 2009, 131 (2)s. 1-11.
13. Heywood, J. B., *Internal Combustion Engine Fundamentals*, McGraw-Hill, New York, 1988.
14. S. M. Aithal, "Development of a Fast, Robust Equilibrium Chemistry Solver for Analyses of Combustion Products," Preprint ANL/MCS-P1825-0111, January 2011
15. S. M. Aithal, "Impact of EGR fraction on diesel engine performance considering heat loss and temperature-dependent properties of the working fluid", *Int. J. Energy Research*. 2008, **33**, 415-430.
16. C. R. Ferguson, A. T. Kirkpatrick, "Internal Combustion Engines: Applied Thermosciences" 2nd Ed, John Wiley and Sons, NY, 2001.
17. <http://navier.engr.colostate.edu/~dandy/code/code-4/index.html>

Table 1: Extended Zeldovich mechanism with rates [13]

	Reaction	K_+	K_-
1	$O + N_2 = NO + N$	$7.6 \times 10^{13} E(-38000/T)$	1.6×10^{13}
2	$N + O_2 = NO + O$	$6.4 \times 10^9 T E(-3150/T)$	$1.5 \times 10^9 T E(-3150/T)$
3	$OH + N = NO + H$	4.1×10^{13}	$2.0 \times 10^{14} E(-23650/T)$

Table 2: Engine dimensions (in mm)

Bore	130
Stroke	140
Compression ratio	11:1
Length of connecting rod	260

Table 3: Operating conditions used in this work

Speed (rpm)	1800
Power (kW)	33
Fuel mass (g)	0.13

ϕ	Air Mass (g)	Spark Timing (θ_i) (CAD)	Combustion Duration (θ_f) (CAD)
1.0	2.23	-22	45
0.9	2.48	-24	48
0.8	2.80	-25	52
0.7	3.2	-30	70
0.65	3.4	-34	78

Table 4: Verification of equilibrium composition of methane-air mixture

	Species	Equilibrium Mole Fraction (Current Study)	STANJAN (Mole Fraction) [17]
1	CH ₄	3.186249E-20	4.8599E-14
2	O ₂	2.043764E-02	2.0456E-02
3	CO ₂	6.579424E-02	6.5726E-02
4	H ₂ O	1.558798E-01	1.5588E-01
5	N ₂	7.015155E-01	7.0157E-01
6	N	1.376168E-06	1.3749E-06
7	O	2.032785E-03	2.0336E-03
8	NO	1.426180E-02	1.4272E-02
9	OH	1.324387E-02	1.3246E-02
10	H	1.582398E-03	1.5815E-03
11	N ₂ O	5.021138E-06	5.0202E-06
12	CO	1.897327E-02	1.8955E-02
13	H ₂	6.228894E-03	6.2259E-03
14	NO ₂	1.703419E-05	1.7034E-05
15	HO ₂	2.639394E-05	2.6397E-05

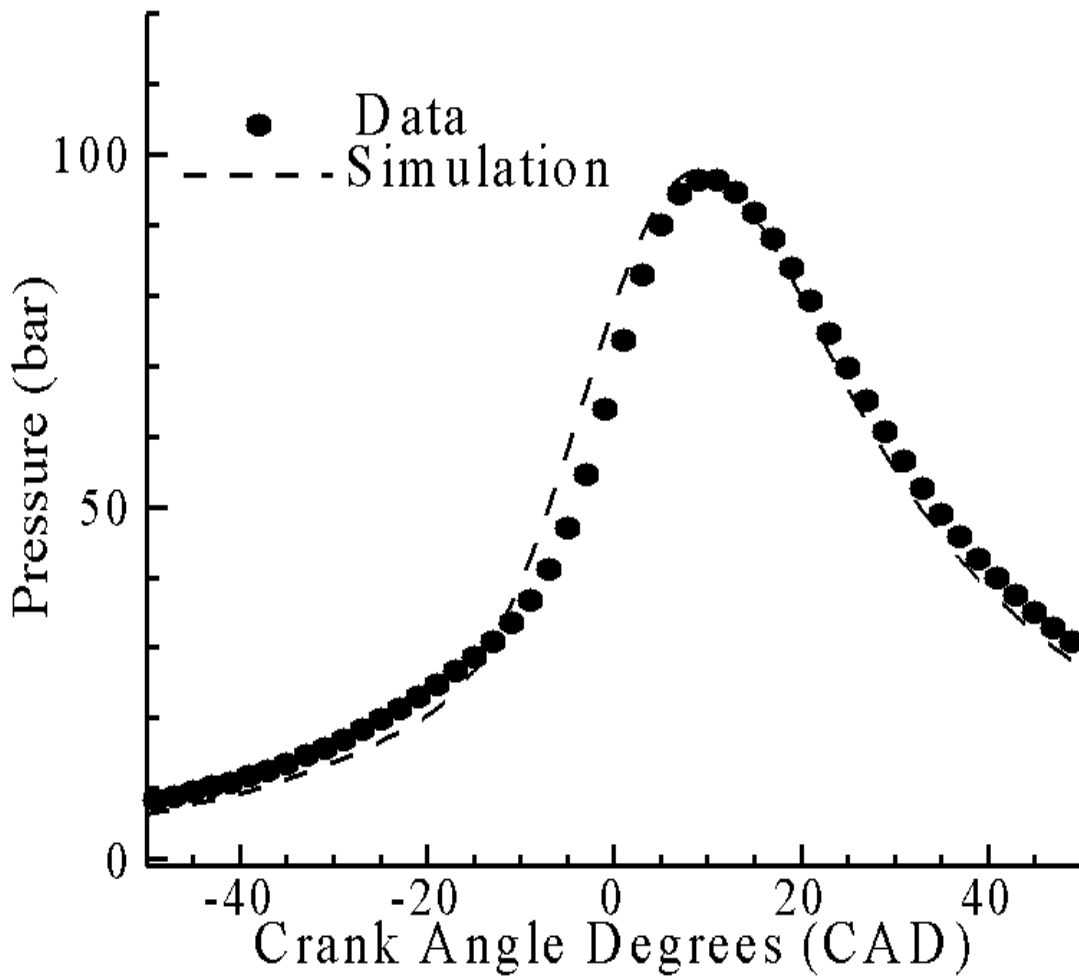


Figure 1: Temporal cylinder pressure (simulation and experimental data).

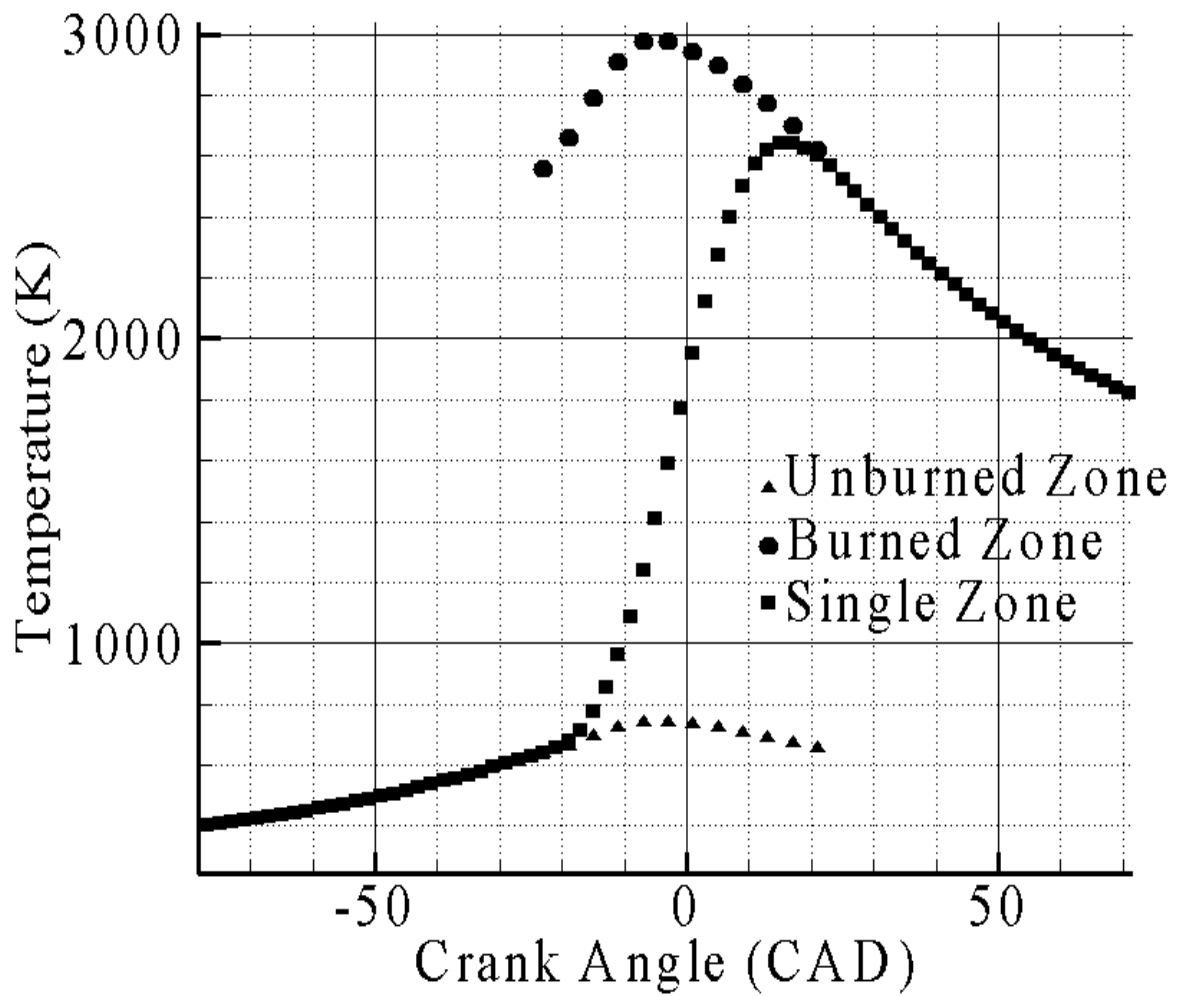


Figure 2: Burned and unburned gas temperatures.

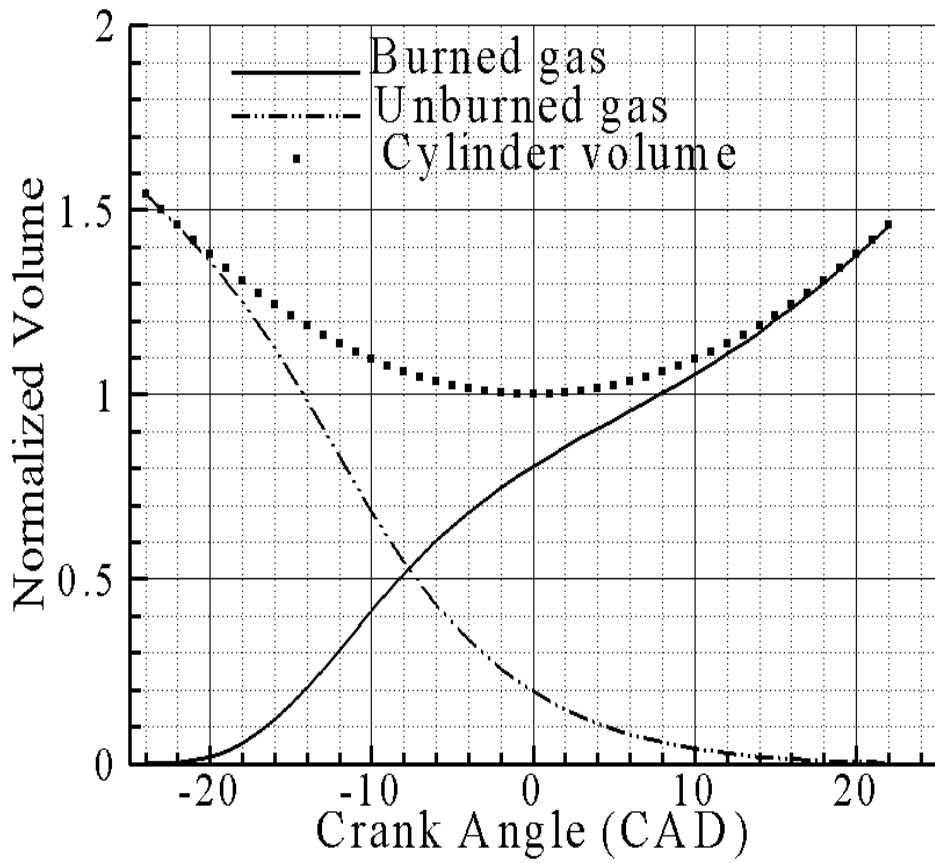


Figure 3: Temporal variation of normalized burned and unburned zone volumes.

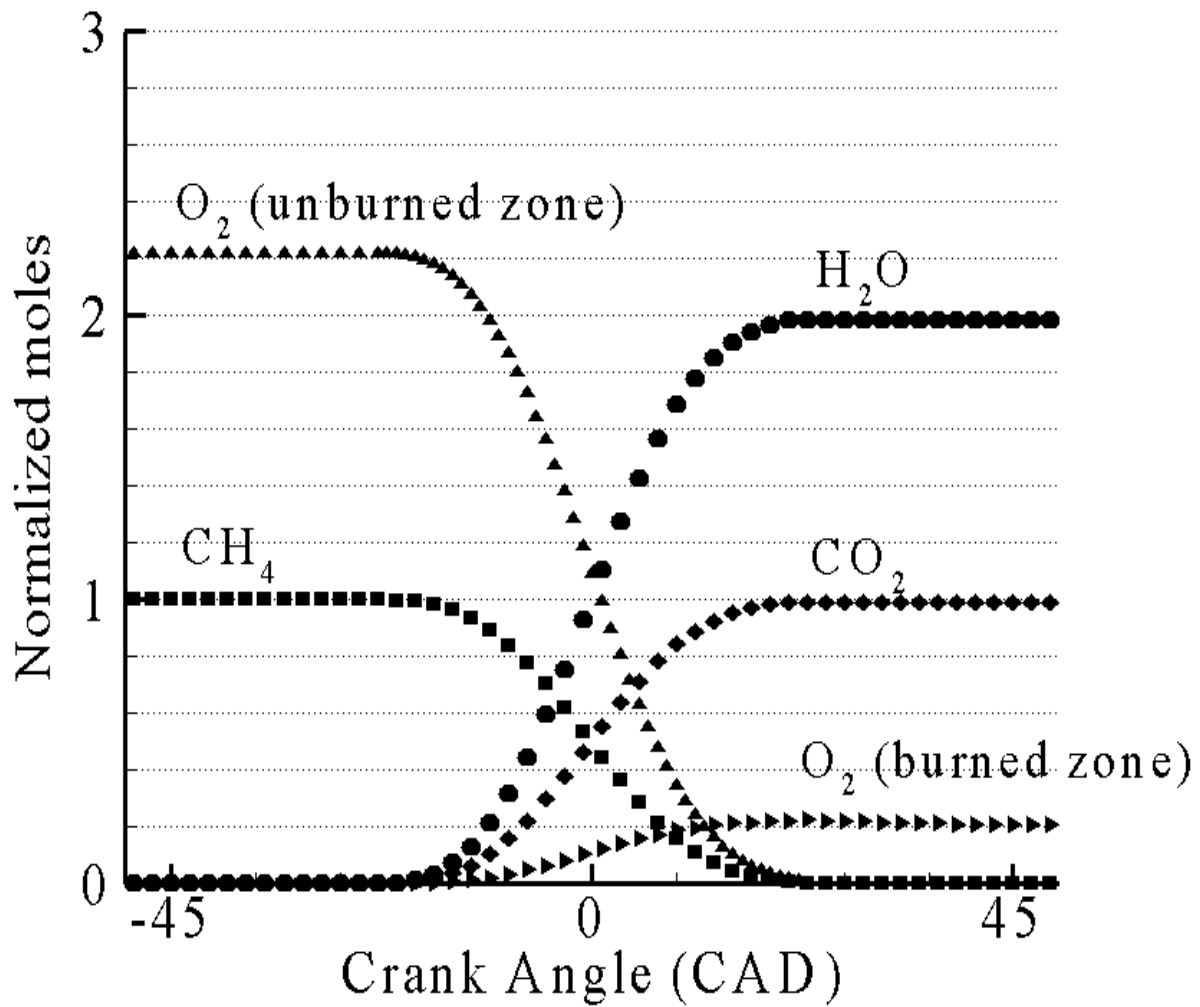


Figure 4: Temporal variation of CH_4 , O_2 , CO_2 and H_2O moles (all species normalized with CH_4 moles).

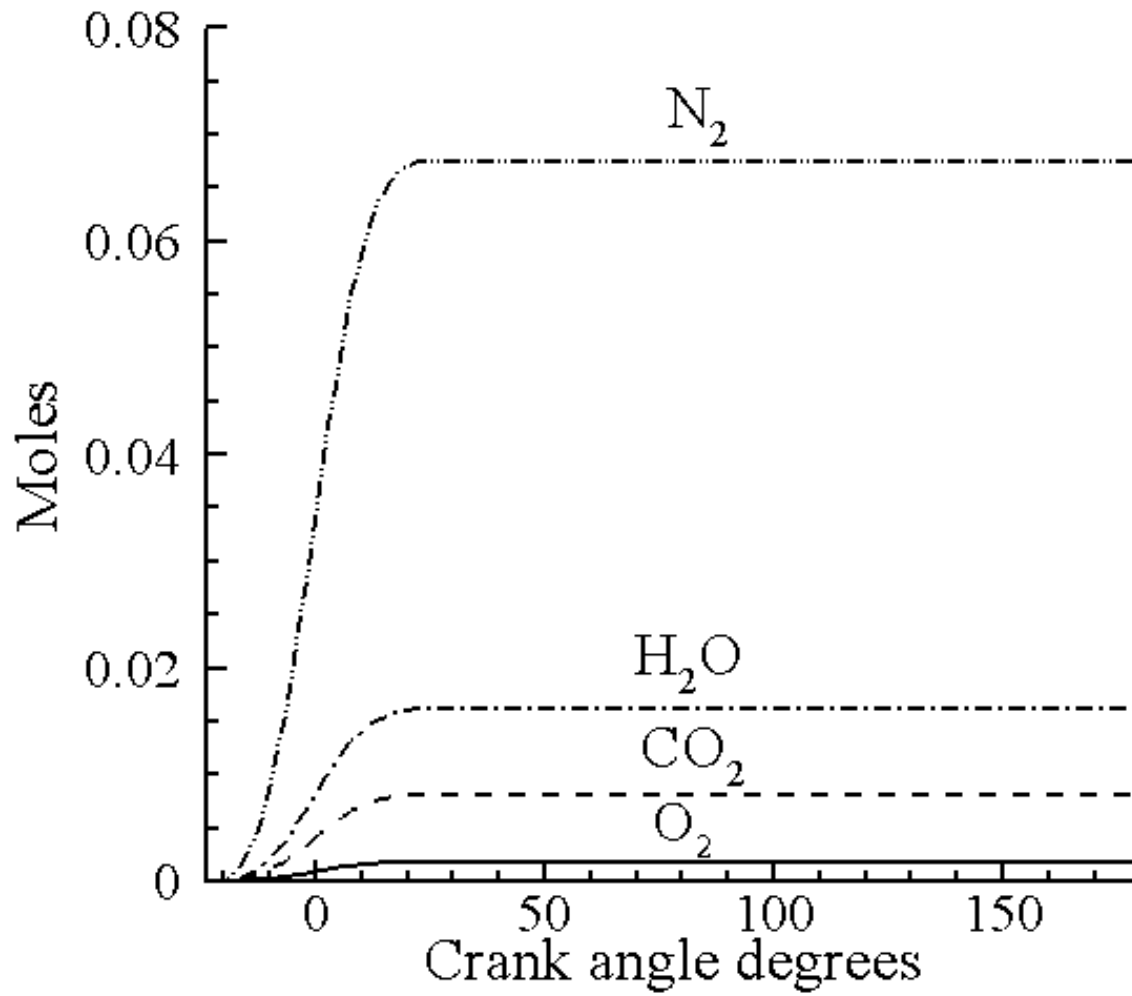


Figure 5: Temporal variation of CO₂, H₂O, O₂ and N₂ moles in the burned zone.

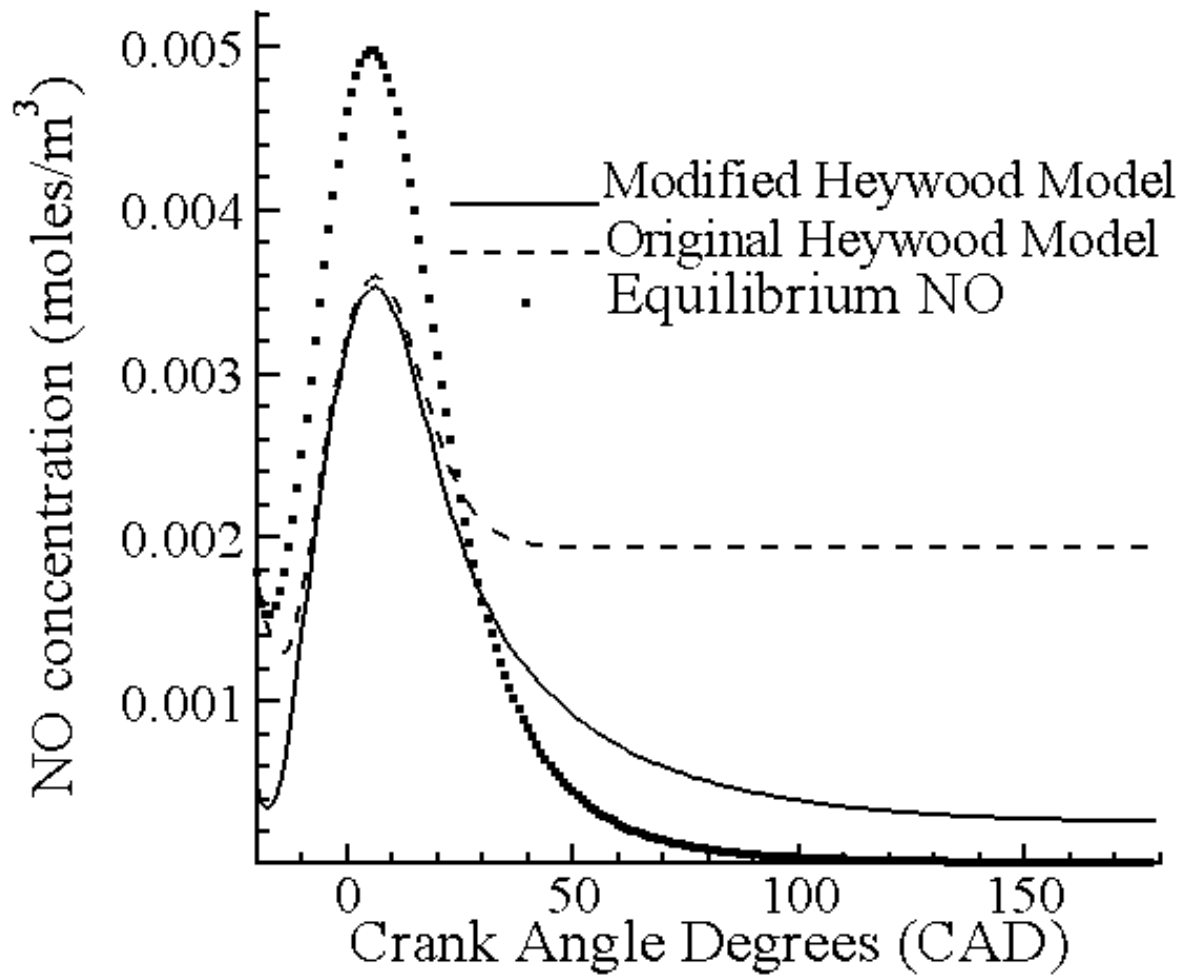


Figure 6: Temporal variation of NO concentration predicted by the original Heywood model, the modified Heywood model and equilibrium chemistry.

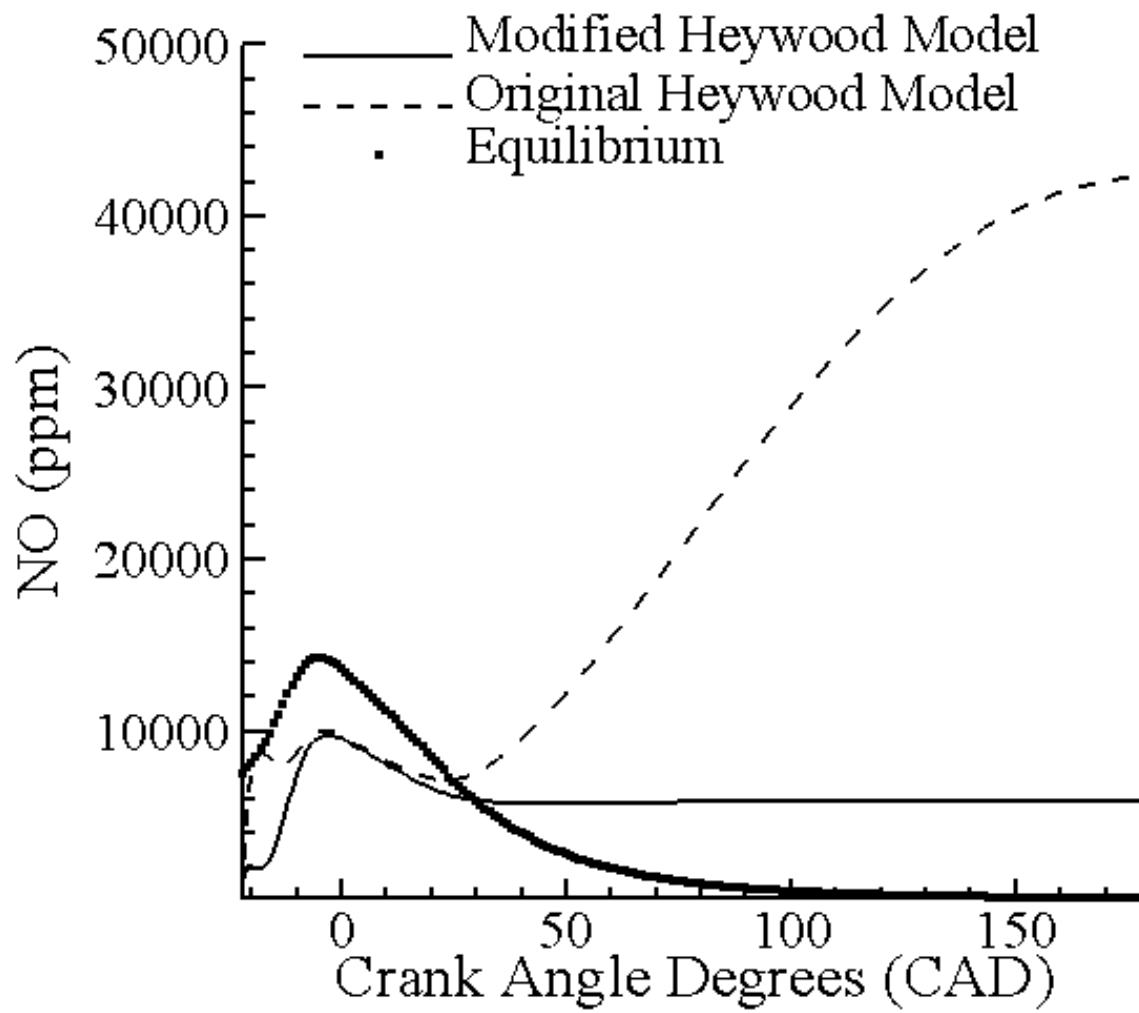


Figure 7: Temporal variation of NO mole fraction (expressed as PPM) predicted by the original Heywood model, the modified Heywood model and equilibrium chemistry.

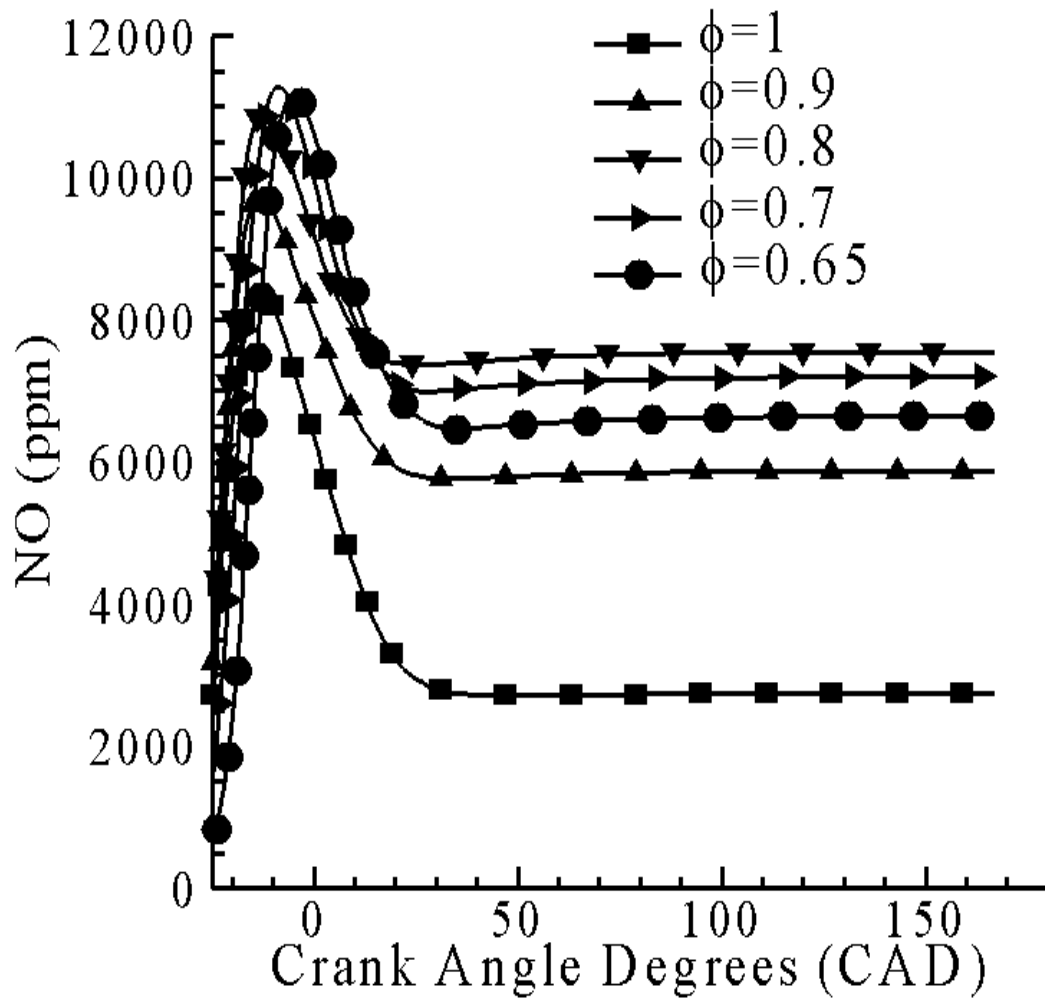


Figure 8: Temporal variation of NO moles fraction (in PPM) for various equivalence ratios using the modified Heywood model.

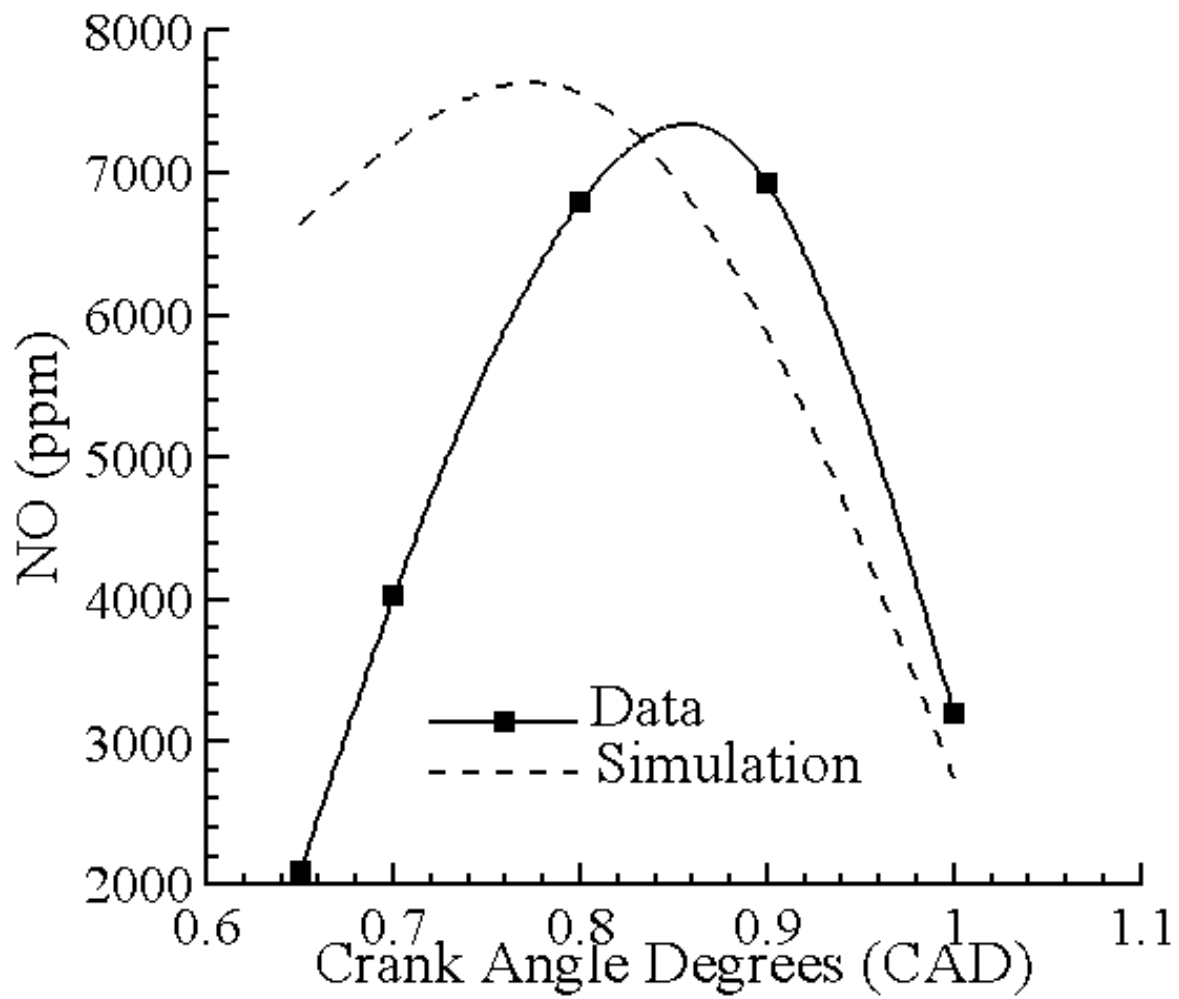


Figure 9: Comparison of predicted engine-out NO with experimental data for various equivalence ratios.

List of Tables

Table 1: Extended Zeldovich mechanism with rates [13]

Table 2: Engine dimensions (in mm)

Table 3: Operating conditions used in this work

Table 4: Verification of equilibrium composition of methane-air mixture.

List of figures:

Figure 1: Temporal cylinder pressure (simulation and experimental data).

Figure 2: Burned and unburned gas temperatures.

Figure 3: Temporal variation of normalized burned and unburned zone volumes.

Figure 4: Temporal variation of CH₄, O₂, CO₂ and H₂O moles (all species normalized with CH₄ moles).

Figure 5: Temporal variation of CO₂, H₂O, O₂ and N₂ moles in the burned zone.

Figure 6: Temporal variation of NO concentration predicted by the original Heywood model, the modified Heywood model and equilibrium chemistry.

Figure 7: Temporal variation of NO mole fraction (expressed as PPM) predicted by the original Heywood model, the modified Heywood model and equilibrium chemistry.

Figure 8: Temporal variation of NO moles fraction (in PPM) for various equivalence ratios using the modified Heywood model.

Figure 9: Comparison of predicted engine-out NO with experimental data for various equivalence ratios.

Government License

The submitted manuscript has been created by UChicago Argonne, LLC, Operator of Argonne National Laboratory ("Argonne"). Argonne, a U.S. Department of Energy Office of Science laboratory, is operated under Contract No. DE-AC02-06CH11357. The U.S. Government retains for itself, and others acting on its behalf, a paid-up nonexclusive, irrevocable worldwide license in said article to reproduce, prepare derivative works, distribute copies to the public, and perform publicly and display publicly, by or on behalf of the Government.